Inorg. Chem. **2004**, *43*, 227–236

Cooperative Spin Crossover and Order–Disorder Phenomena in a Mononuclear Compound [Fe(DAPP)(abpt)]$(ClO_4)_2$ [DAPP = [Bis(3-aminopropyl)(2-pyridylmethyl)amine], abpt = 4-Amino-3,5-bis(pyridin-2-yl)-1,2,4-triazole]

Galina S. Matouzenko,*,† Azzedine Bousseksou,‡ Serguei A. Borshch,† Monique Perrin,§ Samir Zein,† Lionel Salmon,‡ Gabor Molnar,‡ and Sylvain Lecocq§

Laboratoire de Chimie (UMR CNRS and ENS-Lyon No. 5182), École Normale Supérieure de Lyon, 46, allée d'Italie, 69364 Lyon cedex 07, France, Laboratoire de Chimie de Coordination (UPR CNRS No. 8241), 205, route de Narbonne, 31077 Toulouse cedex, France, and Laboratoire de Reconnaissance et Organisation Moléculaire (UMR No. 5078), Université Claude Bernard-Lyon 1, 69622 Villeurbanne cedex, France

Received April 29, 2003

The synthesis and detailed characterization of the new spin crossover mononuclear complex [Fe^{II}(DAPP)(abpt)]-$(ClO_4)_2$, where DAPP = [bis(3-aminopropyl)(2-pyridylmethyl)amine] and abpt = 4-amino-3,5-bis(pyridin-2-yl)-1,2,4-triazole, are reported. Variable-temperature magnetic susceptibility measurements and Mössbauer spectroscopy have revealed the occurrence of an abrupt spin transition with a hysteresis loop. The hysteresis width derived from magnetic susceptibility measurements is 10 K, the transition being centered at $T_c\downarrow = 171$ K for decreasing and $T_c\uparrow = 181$ K for increasing temperatures. The crystal structure was resolved in the high-spin (293 and 183 K) and low-spin (123 K) states. Both spin-state structures belong to the monoclinic space group $P2_1/n$ ($Z = 4$). The thermal spin transition is accompanied by the shortening of the mean Fe–N distances by 0.177 Å. The two main structural characteristics of [Fe(DAPP)(abpt)]$(ClO_4)_2$ are a branched network of intermolecular links in the crystal lattice and the occurrence of two types of order–disorder transitions (in the DAPP ligand and in the perchlorate anions) accompanying the thermal spin change. These features are discussed relative to the magnetic properties of the complex. The electronic structure calculations show that the structural disorder in the DAPP ligand modulates the energy gap between the HS and LS states. In line with previous studies, the order–disorder phenomena and the spin transition in [Fe(DAPP)(abpt)]$(ClO_4)_2$ are found to be interrelated.

Introduction

The phenomenon of spin crossover between low-spin (LS) and high-spin (HS) electronic states was extensively studied during a few past decades and the results have been summarized in several reviews.[1] Its theoretical and experimental aspects, as well as its potential applications, condition a steady interest in this phenomenon. Spin transition is most commonly observed for iron(II) complexes with the nitrogen donor atoms and represents an example of molecular bistability (HS, $S = 2$, $^5T_2 \leftrightarrow$ LS, $S = 0$, $^1A_1$).[2] A bistable behavior underlies the design of new molecular materials for electronic technology[1e,f,h,2] and can be induced by a variation of temperature, pressure, light irradiation, or by magnetic field. To be used in active elements of memory devices, spin transition must be abrupt with a relatively large thermal hysteresis, centered near to ambient temperature.

* Corresponding author. E-mail: Galina.Matouzenko@ens-lyon.fr.
† École Normale Supérieure de Lyon.
‡ Laboratoire de Chimie de Coordination.
§ Université Claude Bernard-Lyon 1.

(1) (a) Goodwin, H. A. *Coord. Chem. Rev.* **1976**, *18*, 293. (b) Gütlich, P. *Struct. Bonding* **1981**, *44*, 83. (c) König, E.; Ritter, G.; Kulshreshtha, S. K. *Chem. Rev.* **1985**, *85*, 219. (d) Toftlund, H. *Coord. Chem. Rev.* **1989**, *94*, 67. (e) Gütlich, P.; Hauser, A. *Coord. Chem. Rev.* **1990**, *97*, 1. (f) Zarembowitch, J.; Kahn, O. *New J. Chem.* **1991**, *15*, 181. (g) König, E. *Struct. Bonding* **1991**, *76*, 51. (h) Gütlich, P.; Hauser, A.; Spiering, H. *Angew. Chem., Int. Ed. Engl.* **1994**, *33*, 2024. (i) Kahn, O. *Molecular Magnetism*; VCH: New York 1993. (j) Real, J. A. In *Transition Metals in Supramolecular Chemistry*; Sauvage, J. P., Ed.; John Wiley & Sons Ltd.: New York, 1999. (k) Sorai, M. *Bull. Chem. Soc. Jpn.* **2001**, *74*, 2223.
(2) (a) Kahn, O.; Launay, J. P. *Chemtronics* **1988**, *3*, 140. (b) Kahn, O.; Kröber, J.; Jay, C. *Adv. Mater.* **1992**, *4*, 718.

10.1021/ic034450e CCC: $27.50
Published on Web 11/25/2003

Chart 1. Representation of the DAPP and Abpt Ligands

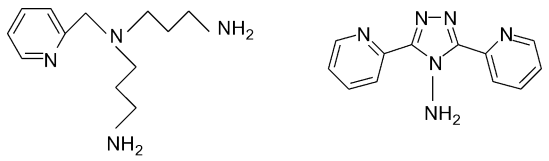

DAPP abpt

Such a magnetic behavior is related to cooperative interactions between the active metal sites in the solid state. Different intermolecular interactions (H-bonding, π stacking, van der Waals contacts) holding together the assemblage of the molecules in the crystal were recognized as leading to pronounced cooperative effects. They serve as information transmitters from one molecule to another when the change of the molecular equilibrium geometry, accompanying a spin transition, occurs. However, due to a noncovalent nature of these cooperative interactions, their spreading in the crystal lattice is difficult to control.[3] Recently, the idea that the cooperativity should be more pronounced in compounds in which the metal active sites are covalently linked by chemical bridges was introduced.[4] In this context, two approaches,[5] namely, supramolecular and polymeric, are presently employed to design new cooperative spin crossover systems. Several theoretical models have been proposed to explain the characteristics of spin crossover complexes in the solid state.[6] Nevertheless, the microscopic origin of the cooperativity is not yet fully identified. Certainly, studies of main chemical and structural factors that control the characteristics of particular spin crossover systems are important to gain a deeper insight into the mechanism of spin transition and to design new systems that can be used in molecular electronics.

In the present paper, we describe the detailed characterization of a new spin transition complex [Fe(DAPP)(abpt)]-$(ClO_4)_2$, with DAPP = [bis(3-aminopropyl)(2-pyridylmethyl)-amine] and abpt = 4-amino-3,5-bis(pyridin-2-yl)-1,2,4-triazole (Chart 1). The magnetic susceptibility measurements and Mössbauer spectroscopy displayed a sharp HS $\leftrightarrow$ LS transition with thermal hysteresis. The single-crystal X-ray structure has been determined for both HS (293 and 183 K) and LS (123 K) forms. The two main structural features of [Fe(DAPP)(abpt)]$(ClO_4)_2$, namely, a branched network of intermolecular links in the crystal lattice and two types of order−disorder transitions, will be discussed further in relation to the spin transition properties of the complex. The results of the electronic structure calculations are used to elucidate the role of the order−disorder phenomenon in the DAPP ligand.

Experimental Section

Chemistry. All reagents and solvents used in this study are commercially available and were used without further purification. All syntheses involving Fe(II) species were carried out in deoxygenated solvents under an inert atmosphere of N_2 using glovebox techniques. The abpt ligand was obtained from the Aldrich Chemical Co. ^{1}H NMR spectra were recorded in $CDCl_3$ on a Bruker AC200 spectrometer operating at 200 MHz. Elemental analyses (C, H, N, Cl, and Fe determination) were performed at the Service Central de Microanalyse du CNRS in Vernaison.

Ligand Synthesis. [Bis(3-aminopropyl)(2-pyridylmethyl)amine] (DAPP) described previously[7] was synthesized using a different procedure. A mixture of 2-(aminomethyl)pyridine (3.2 g, 0.03 mol), triethylamine (8.4 mL, 0.06 mol), and *N*-(3-bromopropyl)phthalimide (16.1 g, 0.06 mol) in toluene (50 mL) was refluxed under argon overnight. Then the resulting precipitate was filtered off and the filtrate was concentrated under vacuum. The solid residue was washed with ether and then recrystallized from the ethanol to give 8.1 g (56%) of [bis(*N*-phthaloyl-3-propyl)(2-pyridylmethyl)]amine as a light beige solid. ^{1}H NMR ($CDCl_3$): δ 8.41−7.02 (m, 4H, pyridinic aromatic H's), 7.81−7.64 (m, 8H, phthalyl aromatic H's), 3.73−3.66 (m, 6H, CH_2), 2.60−2.53 (t, 4H, CH_2), 1.90−1.76 (m, 4H, CH_2). To this product dissolved in 50 mL of absolute ethanol was added 1.63 mL (0.036 mol) of hydrazine monohydrate. The mixture was refluxed under argon until formation of a white gelatinous precipitate. When the formation of the latter appeared complete, it was decomposed by heating with 12 M HCl (15 mL). The precipitate (phthalyl hydrazide hydrochloride) was filtered off and washed with ethanol and water, and then the filtrate was concentrated under vacuum. The residue was made basic with aqueous NaOH, and the organic material was extracted with ether. The ethereal solution was dried over NaOH pellets and evaporated under vacuum to give 2.6 g (70%) of essentially pure DAPP (light yellow oil). ^{1}H NMR ($CDCl_3$): δ 8.48−7.06 (m, 4H, aromatic H's), 3.66 (s, 2H, CH_2), 2.70−2.63 (t, 4H, CH_2), 2.52−2.45 (t, 4H, CH_2), 1.65−1.51 (m, 4H, CH_2), 1.19 (s, 4H, NH_2).

Synthesis of the Iron(II) Complex. A 54.4 mg (0.15 mmol) sample of $Fe(ClO_4)_2 \cdot 6H_2O$ was dissolved in 2 mL of ethanol/methanol (1:1 mixture), and a 33.3 mg (0.15 mmol) sample of DAPP in 2 mL of the same mixture of alcohols was added. A light yellow solution was formed. The addition of 17.9 mg (0.075 mmol) of the abpt ligand in 5 mL of methanol turned the color of this solution to red orange. The deficiency in the abpt ligand was used in order to avoid a partial precipitation of a red solid (1:3 iron to abpt compound). The solution was filtered and allowed to stand overnight at room temperature to give yellow brown crystals of [Fe(DAPP)(abpt)]$(ClO_4)_2$, which were collected by filtration, washed with ethanol, and dried in a vacuum. The crystal used in the X-ray structure determination was selected from this sample. Anal. Calcd for $C_{24}H_{32}N_{10}Cl_2O_8Fe$: C, 40.30; H, 4.51; N, 19.58; Cl, 9.91; Fe, 7.81. Found: C, 40.11; H, 4.63; N, 19.42; Cl, 10.12; Fe, 7.92.

CAUTION! The perchlorate salts of metal complexes with organic ligands are potentially explosive. Only small quantities of

(3) (a) Matouzenko, G. S.; Bousseksou, A.; Lecocq, S.; Koningsbruggen, P. J. v.; Perrin, M.; Kahn, O.; Collet, A. *Inorg. Chem.* **1997**, *36*, 5869. (b) Matouzenko, G. S.; Létard, J.-F.; Bousseksou, A.; Lecocq, S.; Capes, L.; Salmon, L.; Perrin, M.; Kahn, O.; Collet, A. *Eur. J. Inorg. Chem.* **2001**, *11*, 2935.

(4) (a) Kahn, O.; Codjovi, E. *Philos. Trans. R. Soc. London A* **1996**, *354*, 359. (b) Kahn, O.; Garcia, Y.; Létard, J. F.; Mathonière, C. *NATO ASI Ser. C* **1998**, *518*, 127.

(5) Garcia, Y.; Kahn, O.; Rabardel, L.; Chansou, B.; Salmon, L.; Tuchagues, J. P. *Inorg. Chem.* **1999**, *38*, 4663.

(6) (a) Slichter, C. P.; Drickamer, H. G. *J. Chem. Phys.* **1972**, *56*, 2142. (b) Zimmermann, R.; König, E. *J. Phys. Chem. Solids* **1977**, *38*, 779. (c) Rao, P. S.; Ganguli, P.; McGarvey B. R. *Inorg. Chem.* **1981**, *20*, 3682. (d) Sasaki, N.; Kambara, T. *J. Chem. Phys.* **1981**, *74*, 3472. (e) Ohnishi, S. Sugano, S. *J. Phys. C* **1981**, *14*, 39. (f) Spiering, H.; Meissner, E.; Köhler C. P.; Müller E. F.; Gutlich, P. *Chem. Phys.* **1982**, *68*, 65. (g) Spiering, H.; Willenbacher, N. *J. Phys. Condens. Matter* **1989**, 10089.

(7) (a) Adams, H.; Bailey, N. A.; Carlisle, W. D.; Fenton, D. E.; Rossi, G. *J. Chem. Soc., Dalton. Trans.* **1990**, 1271. (b) Hay, R. W.; Clifford, T.; Lightfoot, P. *Polyhedron* **1998**, *17*, 4347.

Table 1. Crystallographic Data for $[Fe(DAPP)(abpt)](ClO_4)_2$

	$T = 293$ K	$T = 183$ K	$T = 123$ K
chem formula		$C_{24}H_{32}N_{10}Cl_2O_8Fe$	
fw		715.35	
a, Å	9.425(2)	9.406(2)	9.511(5)
b, Å	26.526(5)	26.224(5)	27.216(2)
c, Å	12.409(3)	12.338(3)	11.476(6)
β, deg	97.79(3)	98.08(3)	101.07(4)
V, Å^3	3074(1)	3013(1)	2915.3(3)
Z	4	4	4
space group	$P2_1/n$	$P2_1/n$	$P2_1/n$
λ, Å	0.71070	0.71070	0.71070
ρ_{calc}, g·cm^{-3}	1.546	1.577	1.630
μ, cm^{-1}	7.28	7.43	7.70
R^a [$I > 2\sigma(I)$]	0.074	0.080	0.071
$wR_2{}^b$ [$I > 2\sigma(I)$]	0.182	0.209	0.149

$^a R = \sum(|F_o| - |F_c|)/\sum|F_o|$. $^b wR_2 = \{\sum[w(F_o^2 - F_c^2)^2]/\sum[w(F_o^2)^2]\}^{1/2}$.

the compound should be prepared, and they should be handled with much care!

Physical Measurements. Magnetic Properties. Variable-temperature magnetic susceptibility data were obtained on a polycrystalline sample with a Faraday-type magnetometer equipped with a continuous-flow Oxford Instruments cryostat. Diamagnetic corrections were applied by using Pascal's constants.

Mössbauer Spectra. The variable-temperature Mössbauer measurements were performed on a constant-acceleration spectrometer with a 50 mCi source of ^{57}Co (Rh matrix). The isomer shift values (δ) are given with respect to metallic iron at room temperature. The absorber was a sample of microcrystalline powder enclosed in a 2 cm diameter cylindrical plastic sample holder, the size of which had been determined to optimize the absorption. Spectra were obtained in the range 80−305 K, by using a MD306 Oxford cryostat, the thermal scanning being monitored by an Oxford ITC4 servocontrol device (±0.1 K). A least-squares computer program[8] was used to fit the Mössbauer parameters and to determine their error bars of statistical origin (given in parentheses).

Solution and Refinement of the X-ray Structure. A Nonius Kappa CCD diffractometer was used for data collection. The selected crystals were mounted on a thin glass fiber. Three collections were made: the first one at room temperature, the second one at 183 K after a slow decrease of the temperature with a cool dry nitrogen gas stream, and the third one at 123 K just after a sudden cooling of the crystal by a cold nitrogen gas flow. From 10 frames with 1° steps, the initial set of cell parameters was obtained for each measurement. A total of 26595 reflections were collected at room temperature of which 6976 unique reflections were used for the structure determination. The second collection at 183 K is formed from 23686 measured reflections, 4582 of which were independent reflections. The third collection at 123 K concerns 24730 measured reflections, of which 6463 unique reflections were used for the hypothesis and refinement. The structures were solved by direct method with the SHELXS-97 program.[9] Then the structures were refined by the least-squares method using SHELXL-97[10] with anisotropic temperature factors for all non-H atoms. The hydrogen atoms were introduced at calculated positions and refined riding on their carrier atoms. The same procedure was applied for the oxygen atoms at 293 K. The final R factor (with $I > 2\sigma(I)$) has a value of 0.074, 0.080, and 0.071 for 293, 183, and 123 K, respectively. Crystal data and refinement results are summarized in Table 1. The perspective view of the asymmetric unit at three temperatures has been calculated with PLATON[11] and is shown in Figure 1.

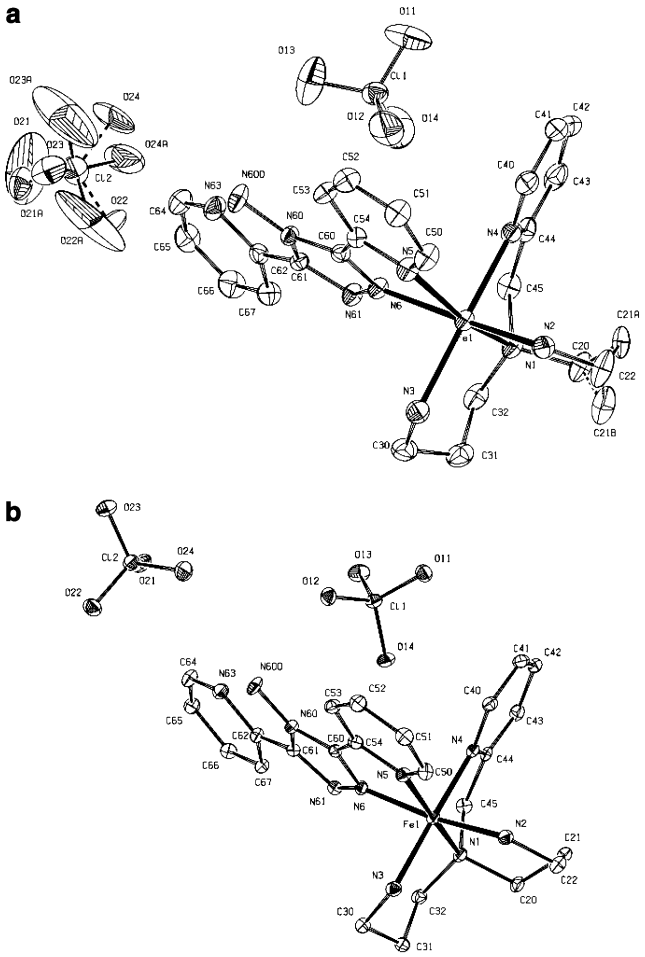

Figure 1. ORTEP view of the $[Fe(DAPP)(abpt)](ClO_4)_2$ molecule at 293 K (a) and 123 K (b). Ellipsoids enclose 20% probability.

Electronic Structure Calculations. DFT calculations of the complex cation $[Fe(DAPP)(abpt)]^{2+}$ were performed using the Gaussian 98 package.[12] Single-point calculations were done at the experimental geometry found at 293 and 123 K. Both LS and HS states were considered for each structure. In all calculations the Dunning−Huzinaga double-ζ basis set for H, C, and N and the Los Alamos effective core potential plus double-ζ basis for Fe were used.[13] Following the previous studies of spin transition complexes,

(8) Varret, F. *Proceedings of the International Conference on Mössbauer Effect Applications*, Jaipar, India, 1981; Indian National Science Academy: New Delhi, 1982.
(9) Sheldrick, G. M. *SHELXS-97, Program for Crystal Structure Determination*; University of Göttingen: Göttingen, Germany, 1997.
(10) Sheldrick, G. M. *SHELXL-97, Program for Crystal Structure Refinement*; University of Göttingen: Göttingen, Germany, 1997.
(11) Spek, A. L. *PLATON, A Multipurpose Crystallographic Tool*; Utrecht University: Utrecht, The Netherlands, 1999.
(12) Frisch, M. J.; Trucks, G. W.; Schlegel, H. B.; Scuseria, G. E.; Robb, M. A.; Cheeseman, J. R.; Zakrzewski, V. G.; Montgomery, J. A.; Stratmann, R. E.; Buran, J. C.; Dapprich, S.; Millam, J. M.; Daniels, A. D.; Kudin, K. N.; Strain, M. C.; Farkas, O.; Tomasi, J.; Barone, V.; Cossi, M.; Cammi, R.; Mennuci, B.; Pomelli, C.; Adamo, C.; Clifford, S.; Ochterski, J.; Peterson, G. A.; Ayala, P. Y.; Cui, Q.; Morokuma, K.; Malick, D. K.; Rabuk, A. D.; Raghavachari, K.; Foresman, J. B.; Cioslowski, J.; Ortiz, J. V.; Stefanov, B. B.; Liu, G.; Liashenko, A.; Piskorz, P.; Komaromi, I.; Gomperts, R.; Martin, R. L.; Fox, D. J.; Keith, T.; Al-Laham, M. A.; Peng, C. Y.; Nanayakkara, A.; Gonzalez, C.; Challacombe, M.; Gill, P. M. W.; Johnson, B. G.; Chen, W.; Wong, M. W.; Andres, J. L.; Head-Gordon, M.; Replogle, E. S.; Pople, J. A. *Gaussian 98*, revision A.7; Gaussian, Inc.: Pittsburgh, PA, 1998.

Table 2. Selected Bond Distances (Å) for $[Fe(DAPP)(abpt)](ClO_4)_2$[a]

	$T = 293$ K	$T = 183$ K	$T = 123$ K
Fe(1)−N(1)	2.233(3)	2.206(5)	2.077(3)
Fe(1)−N(2)	2.167(3)	2.151(5)	2.040(4)
Fe(1)−N(3)	2.178(4)	2.162(5)	2.027(3)
Fe(1)−N(4)	2.179(4)	2.158(5)	1.977(3)
Fe(1)−N(5)	2.252(3)	2.223(5)	2.028(3)
Fe(1)−N(6)	2.184(3)	2.158(4)	1.983(3)

[a] Estimated standard deviations in the least significant digits are given in parentheses.

Table 3. Selected Angles (deg) for $[Fe(DAPP)(abpt)](ClO_4)_2$[a]

	$T = 293$ K	$T = 183$ K	$T = 123$ K
N(1)−Fe(1)−N(2)	95.3(2)	95.6(2)	94.8(1)
N(1)−Fe(1)−N(3)	95.2(2)	95.6(2)	94.3(1)
N(1)−Fe(1)−N(4)	77.4(2)	78.1(2)	83.1(1)
N(1)−Fe(1)−N(5)	163.2(2)	163.9(2)	173.9(1)
N(1)−Fe(1)−N(6)	93.5(2)	93.2(2)	94.6(1)
N(2)−Fe(1)−N(3)	92.7(2)	92.0(2)	91.8(1)
N(2)−Fe(1)−N(4)	91.5(2)	91.0(2)	88.4(1)
N(2)−Fe(1)−N(5)	97.0(2)	96.4(2)	89.9(1)
N(2)−Fe(1)−N(6)	171.2(2)	171.2(2)	169.7(1)
N(3)−Fe(1)−N(4)	171.8(2)	173.2(2)	177.4(1)
N(3)−Fe(1)−N(5)	95.5(2)	94.7(2)	89.5(1)
N(3)−Fe(1)−N(6)	87.3(2)	87.2(2)	91.8(1)
N(4)−Fe(1)−N(5)	90.9(2)	91.0(2)	93.1(1)
N(4)−Fe(1)−N(6)	89.6(2)	90.7(2)	88.5(1)
N(5)−Fe(1)−N(6)	74.2(2)	74.9(2)	80.5(1)

[a] Estimated standard deviations in the least significant digits are given in parentheses.

four DFT methods were used: (i) Perdew and Wang exchange and gradient corrected correlation functionals (PW 91),[14] (ii) Becke exchange and Lee, Yang, and Parr correlation functionals (BLYP method),[15] (iii) hybrid three-member exchange-correlation functional (B3LYP method),[16] (iv) recently proposed reparametrized functional, differing from B3LYP by the coefficient for the Hartree−Fock exchange.[17] As the splitting between spin multiplets presents a rather small difference of two total energies, the convergence cycles were continued until the difference between two successive cycles was $<10^{-8}$ for the electronic density and $<10^{-6}$ for the total energy.

Results

Description of the Structure. The single-crystal X-ray structure of $[Fe(DAPP)(abpt)](ClO_4)_2$ was determined in the HS (293 and 183 K) and LS (123 K) states. Both spin state isomers adopt the monoclinic space group $P2_1/n$ with $Z = 4$. Selected bond lengths and angles for the two spin state forms are given in Tables 2 and 3, respectively. The distorted octahedral coordination sphere of the iron(II) atom is formed by six nitrogen atoms belonging to the abpt and DAPP ligands (Figure 1). The potentially bis-bidentate abpt ligand, actually acting as a bidentate one, is coordinated to iron(II) in *cis*-position by one pyridyl and one triazole nitrogens. The four remaining positions in the $[FeN_6]$ core are occupied by one pyridinic and three aliphatic nitrogen atoms of the DAPP ligand. The latter forms with iron(II) one five-membered and two six-membered chelate metallocycles. It can be noted that two primary aliphatic amino groups of the DAPP ligand can have either a facial or meridional arrangement leading in principle to a number of isomers. The *mer* configuration is achiral (due to the flexibility of the six-membered rings) whereas the *fac* arrangement leads to a chiral complex. Moreover, two possible opposite orientations of noncoordinated nitrogen atoms of the abpt ligand relative to the DAPP ligand can give an additional number of isomers. In $[Fe(DAPP)(abpt)](ClO_4)_2$, the DAPP ligand adopts a chiral *fac* configuration and the unit cell contains two pairs of symmetry related left-handed and right-handed enantiomers.

(a) High-Spin Complex Structure. $T = 293$ K. Among the Fe−N distances involving the DAPP ligand, the Fe−N1 distance (2.233(3) Å) is considerably longer than three others which are close and fall within 2.167(3)−2.179(4) Å (see Table 2). Concerning the Fe−N(abpt) bond lengths, the Fe−N(pyridine) distance (2.252(3) Å) is significantly longer than the Fe−N(triazole) one (2.184(3) Å). This inequivalence in the Fe−N distances with the abpt ligand was early observed for numerous metal complexes.[18] Thus, the $[FeN_6]$ octahedron in $[Fe(DAPP)(abpt)](ClO_4)_2$ is axially elongated along the N1−Fe−N5 direction. This elongation can be interpreted as a pseudo Jahn−Teller distortion. The N−Fe−N angles between the adjacent and the opposite nitrogen atoms fall within the range 74.2(2)−97.0(2)° and 163.2(2)−171.8(2)°. The largest decrease from 90° is observed in the five-membered metallocycles (Table 3). The N−Fe−N angles in the two six-membered metallocycles are close to the ideal octahedron value, probably due to the flexibility of the amino aliphatic chain.

The configuration of the abpt ligand in the $[Fe(DAPP)(abpt)](ClO_4)_2$ complex is similar to that observed in other mononuclear abpt compounds.[18] The nitrogen atom of the noncoordinated pyridyl group is set in the position appropriate to form an intramolecular hydrogen bond with the amino group, i.e., N600−H60···N63. Both, the bidentate coordination mode and the availability of the intramolecular hydrogen bond result in a near planar configuration of the abpt ligand in the complex.

The two six-membered metallocycles formed by the DAPP ligand adopt different conformations. The FeN1N3C30C31C32 metallocycle has a *chair* conformation. The FeN1N2C20C22 fragment of the second metallocycle is roughly planar whereas the C21 atom occupies two positions (Figure 1a) with the occupancy ratio 0.5:0.5, forming a disordered *half-boat* conformation.[19]

(13) (a) Dunning, T. H., Jr.; Hay, P. J. In *Modern Theoretical Chemistry*; Schaefer, H. F., III, Ed.; Plenum: New York, 1976; Vol. 3, p 1. (b) Hay, P. J.; Wadt, W. R. *J. Chem. Phys.* **1985**, *82*, 270.
(14) Perdew, J. P.; Burke, K.; Wang, Y. *Phys. Rev. B* **1996**, *54*, 16533.
(15) (a) Lee, C.; Yang, W.; Parr, R. G. *Phys. Rev. B* **1988**, *37*, 785. (b) Miehlich, B.; Savin, A.; Stoll, H.; Preuss, H. *Chem. Phys. Lett.* **1989**, *157*, 200.
(16) Becke, A. D. *J. Chem. Phys.* **1993**, *98*, 5648.
(17) Reiher, M. *Inorg. Chem.* **2002**, *41*, 6928.
(18) (a) Faulmann, C.; van Köningsbruggen, P. J.; de Graaff, R. A. G.; Haasnoot, J. G.; Reedijk, J. *Acta Crystallogr., Sect. C* **1990**, *46*, 2357. (b) Cornelissen, J. P.; van Diemen, J. H.; Groeneveld, L. R.; Haasnoot, J. G.; Spek, A. L.; Reedijk, J. *Inorg. Chem.* **1992**, *31*, 198. (c) Kunkeler, P. J.; van Köningsbruggen, P. J.; Cornelissen, J. P.; van der Horst, A. N.; van der Kraan, A. M.; Spek, A. L.; Haasnoot, J. G.; Reedijk, J. *J. Am. Chem. Soc.* **1996**, *118*, 2190. (d) van Königsbruggen, P. J.; Goubitz, K.; Haasnoot, J. G.; Reedijk, J. *Inorg. Chim. Acta* **1998**, *298*, 37. (e) Moliner, N.; Muñoz, M. C.; Létard, J.-F.; Solans, X.; Burriel, R.; Castro, M.; Kahn, O.; Real, J. A. *Inorg. Chim. Acta* **1999**, *291*, 279. (f) Moliner, N.; Gaspar, A. B.; Muñoz, M. C.; Niel, V.; Cano, J.; Réal, J. A. *Inorg. Chem.* **2001**, *40*, 3986.

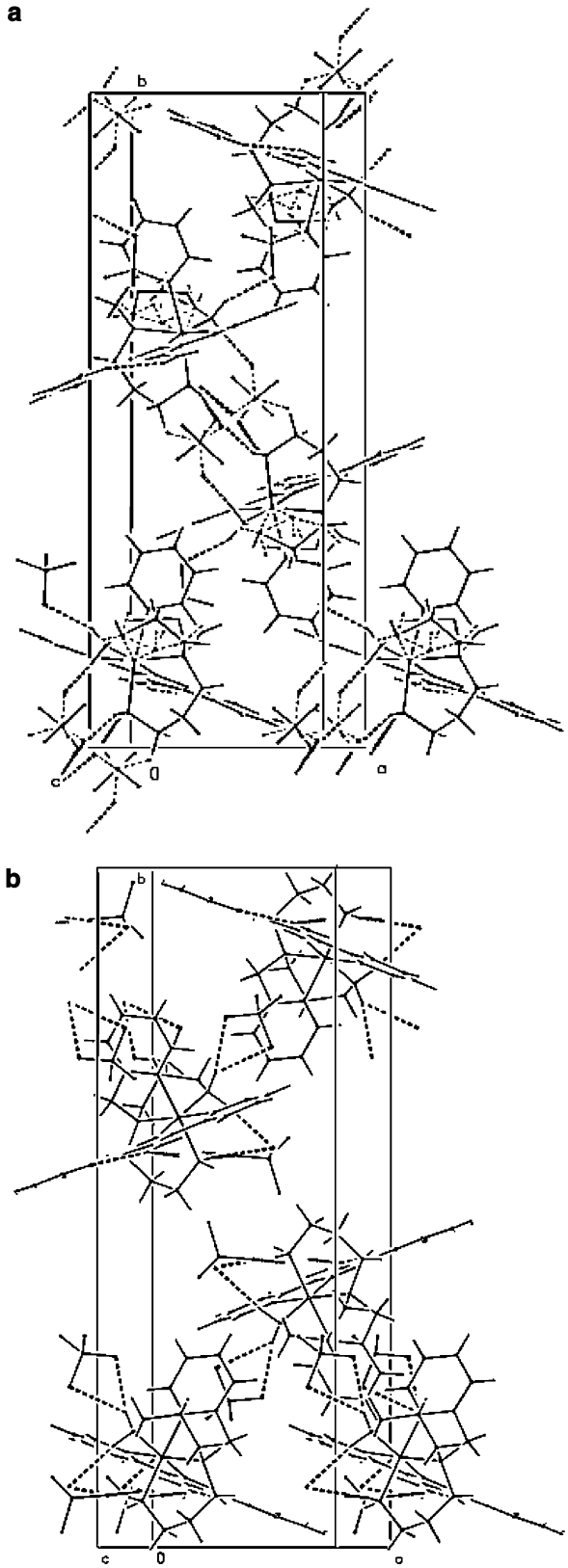

Figure 2. Projection of the molecular structure on the *ab* plane showing the H-bonding network at 293 K (a) and 123 K (b).

Despite relatively increased values of the thermal anisotropic factors, the ClO_4 group with the Cl1 atom is resolved in a single orientation. The perchlorate group involving the Cl2 atom was found to be disordered over two positions (Figure 1a) with close to 0.5:0.5 occupancy. However, the large values of the anisotropic displacement parameter for the O atoms indicate that the disorder model with only two positions for the ClO_4 groups, derived from the SHELXS-97 program, is not fully satisfactory. It may be that at room temperature the perchlorate ions with the Cl2 atom are disordered over several close orientations.

Figure 2a shows a projection of the structure on the *ab* plane. The crystal packing consists of alternate layers along the *b* axis with the antiparallel alignment of the molecules. Each layer is built up from two sheets of molecules related by the symmetry operation $-x, -y, -z$. The disordered Cl2 perchlorate ions are inserted between the sheets of molecules inside a layer, whereas those with the Cl1 atom are localized in the proximity of the neighboring layers. In a layer, the cohesion is achieved by numerous hydrogen bonds (Table 4). The intermolecular H-bonds link molecules from the neighboring sheets indirectly via the oxygen atoms of Cl2 perchlorate ions (Figure 2a). Moreover, the layer molecules are bound by two modes of π stacking interactions (Figure 3), evidenced by short C···C intermolecular distances (Table 5). The first mode arises from a partial overlap between the coordinated and noncoordinated pyridyl rings of the abpt ligands belonging to adjacent molecules from the same sheet

Table 4. Intermolecular C···C Contacts (Å) Shorter Than van der Waals Distances (3.6 Å) for $[Fe(DAPP)(abpt)](ClO_4)_2$[a,b]

	$T = 293$ K	$T = 183$ K	$T = 123$ K
	Mode 1		
C(52)···C(66)[1]	3.509(11)	3.448(10)	3.425(6)
C(52)···C(67)[1]	3.420(10)	3.372(9)	3.519(6)
C(53)···C(66)[1]	3.488(10)	3.403(9)	3.414(6)
C(53)···C(65)[1]			3.570(6)
	Mode 2		
N(63)···C(65)[2]	3.459(10)	3.420(8)	
C(65)···N(63)[2]	3.459(10)	3.420(8)	
C(62)···C(64)[2]			3.422(6)
C(64)···C(62)[2]			3.422(6)
C(62)···C(65)[2]		3.586(8)	
C(65)···C(62)[2]		3.586(8)	
C(64)···C(65)[2]	3.621(11)	3.593(9)	
C(65)···C(64)[2]	3.621(11)	3.593(9)	
C(64)···C(66)[2]	3.537(11)	3.519(10)	
C(66)···C(64)[2]	3.537(11)	3.519(10)	
C(64)···C(67)[2]		3.593(9)	
C(67)···C(64)[2]		3.593(9)	
N(63)···N(63)[2]			3.468(8)

[a] Key: (1) $1 + x, y, z$; (2) $1 - x, -y, 1 - z$. [b] Estimated standard deviations in the least significant digits are given in parentheses.

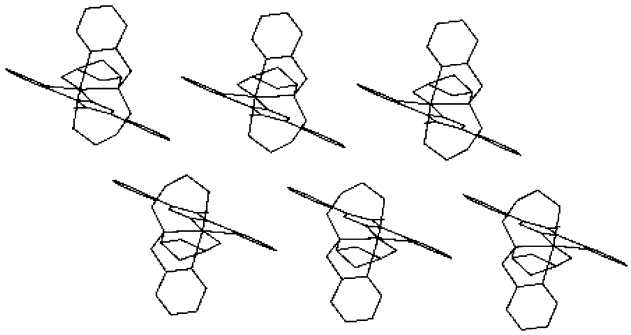

Figure 3. View of $[Fe(DAPP)(abpt)](ClO_4)_2$ showing the π stacking interactions at 293 K.

(19) Cremer, D.; Pople, J. A. *J. Am. Chem. Soc.* **1975**, *97*, 1354.

Table 5. Interatomic Distances (Å) and Angles (deg) for the Hydrogen Bonding Interactions for [Fe(DAPP)(abpt)]$(ClO_4)_2$[a,b]

D−H···A	D−H	H···A	D···A	D−H···A
	293 K			
N(2)−H(2A)···O(11)[1]	0.900	2.196	3.018(7)	151.7
N(2)−H(2B)···O(24)[2]	0.900	2.129	2.959(9)	152.8
N(3)−H(3A)···O(21)[2]	0.900	2.144	2.973(8)	152.8
N(3)−H(3A)···O(21A)[2]	0.900	2.518	3.318(8)	148.3
N(3)−H(3B)···O(21)[3]	0.900	2.477	3.362(9)	168.0
N(3)−H(3B)···O(21A)[3]	0.900	2.333	3.209(9)	164.5
N(600)−H(60B)···O(24A)[4]	0.860	2.600	3.124(9)	120.4
N(600)−H(60B)···N(63)[5]	0.860	2.357	2.905(6)	122.0
C(32)−H(32A)···O(23A)[6]	0.970	2.529	3.411(8)	151.2
C(32)−H(32B)···N(61)[5]	0.970	2.617	3.408(6)	139.0
C(45)−H(45A)···O(11)[1]	0.970	2.545	3.505(7)	170.4
C(45)−H(45B)···N(61)[5]	0.970	2.532	3.331(6)	139.7
C(50)−H(50)···O(11)[1]	0.930	2.455	3.245(6)	142.8
C(53)−H(53)···N(600)[5]	0.930	2.443	3.064(7)	124.2
C(65)−H(65)···O(22A)[5]	0.930	2.145	3.061(8)	168.3
	183 K			
N(2)−H(2A)···O(11)[1]	0.900	2.191	3.005(6)	150.0
N(2)−H(2B)···O(24)[2]	0.900	2.044	2.888(6)	155.7
N(3)−H(3A)···O(21)[2]	0.900	2.352	3.152(6)	148.0
N(3)−H(3B)···O(21)[3]	0.900	2.324	3.197(5)	163.7
N(600)−H(60B)···N(63)[5]	0.860	2.369	2.912(6)	121.5
C(32)−H(32B)···N(61)[5]	0.970	2.577	3.373(6)	139.3
C(45)−H(45A)···O(11)[7]	0.970	2.511	3.472(6)	171.2
C(45)−H(45B)···N(61)[5]	0.970	2.486	3.283(5)	139.4
C(50)−H(50)···O(11)[1]	0.930	2.397	3.216(6)	147.0
C(53)−H(53)···N(600)[5]	0.930	2.429	3.050(5)	124.2
C(66)−H(66)···O(22)[8]	0.930	2.596	3.449(6)	152.6
	123 K			
N(2)−H(2A)···O(11)[1]	0.920	2.537	3.118(5)	121.5
N(2)−H(2A)···O(13)[1]	0.920	2.310	3.170(5)	155.4
N(2)−H(2B)···O(23)[2]	0.920	2.549	3.461(5)	171.3
N(3)−H(3A)···O(21)[2]	0.920	2.228	3.134(5)	168.0
N(3)−H(3A)···O(23)[2]	0.920	2.516	3.202(5)	131.6
N(600)−H(60B)···O(21)[4]	0.880	2.581	2.982(5)	108.7
N(600)−H(60B)···N(63)[5]	0.880	2.378	2.930(5)	121.0
C(32)−H(32B)···N(61)[5]	0.990	2.478	3.269(5)	136.6
C(40)−H(40)···N(5)[5]	0.950	2.624	3.117(5)	112.8
C(43)−H(43)···O(11)[7]	0.950	2.433	3.354(5)	163.3
C(43)−H(43)···O(12)[7]	0.950	2.450	3.204(5)	136.3
C(45)−H(45B)···N(61)[5]	0.990	2.423	3.157(5)	130.5
C(50)−H(50)···N(2)[5]	0.950	2.527	3.041(5)	114.0
C(51)−H(51)···O(14)[4]	0.950	2.571	3.388(5)	144.3
C(52)−H(52)···O(13)[4]	0.950	2.536	3.305(5)	138.2
C(53)−H(53)···N(600)[5]	0.950	2.469	3.077(5)	121.7

[a] Symmetry operations: (1) $-0.5 + x$, $0.5 - y$, $0.5 + z$; (2) $-1 + x$, y, $1 + z$; (3) $1 - x$, $-y$, $1 - z$; (4) $-1 + x$, y, z; (5) x, y, z; (6) x, y, $1 + z$; (7) $0.5 + x$, $0.5 - y$, $0.5 + z$; (8) $2 - x$, $-y$, $1 - z$. [b] Estimated standard deviations in the least significant digits are given in parentheses.

(symmetry operation $-1 + x$, y, z). The dihedral angle between the π stacked pyridyl rings is 5.4(3)°. The second mode, along the *c* direction, links molecules from different sheets inside a layer. It results from the overlapping between parallel aligned noncoordinated pyridyl rings of the abpt ligands (symmetry operation $1 - x$, $-y$, $1 - z$). The distance between the centroids of π stacked pyridyl rings corresponds to 3.625(7) Å. In the *b* direction, the cohesion between the layers is achieved mainly due to van der Waals interactions.

***T* = 183 K (Cooling Mode).** The comparison of the corresponding distances and angles (Tables 2 and 3) shows that the geometry of the $[FeN_6]$ coordination core at 183 K is very close to that at 293 K. The overall conformations of the abpt and DAPP ligands are almost the same at two temperatures. The disorder in the C21 methylene group position in the DAPP ligand is retained also at 183 K. However, the C21A position becomes preferable (refined occupancy ratio 0.7:0.3). At 183 K the difference electron density peaks around the Cl atoms suggest only one favored orientation for each perchlorate anion. The anisotropic thermal parameters for the oxygen atoms for ClO_4 groups are considerably reduced relative to 293 K, remaining, however, higher than those for other atoms. This suggests that the perchlorate ions with the Cl2 atom have undergone an order−disorder transition on going to 183 K.

The crystal packing is identical to that at 293 K. Upon lowering the temperature to 183 K the lattice parameters decrease and the crystal structure becomes more compact. The volume of the unit cell is reduced by 2.0% (60 Å^3). The thermal contraction of the cell parameters is associated with some shortening of the bond lengths (Table 2). The network of the intermolecular interactions is similar to that found at room temperature (Figure 2a). However, the intermolecular distances connected with H-bonding (Table 4) and π stacking (Table 5) are appreciably reduced, showing the strengthening of the intermolecular interactions upon cooling.

(b) Low-Spin Complex Structure. *T* = 123 K. The comparison of the HS and LS complex structures reveals several differences between them. As it could be expected, the HS → LS transition is accompanied by a shortening of the metal−ligand distances. The reduction of the Fe−N(abpt) distance in the LS complex is important and equals 0.224 Å (Fe−N5) and 0.201 Å (Fe−N6) relative to the HS form at room temperature. The Fe−N(DAPP) bond lengths are shorter by 0.156 Å (Fe−N1), 0.127 Å (Fe−N2), 0.151 Å (Fe−N3), and 0.202 Å (Fe−N4). The Fe−N bond lengths as well as the N−Fe−N angles (Tables 2 and 3), show that the HS → LS transition results in a more regular octahedral geometry of the $[FeN_6]$ core. The two six-membered metallocycles formed by the DAPP ligand retain their different *chair* and *half-boat* conformations.

Another important feature is the regular arrangement of the C21 methylene group. This implies the occurrence of the order−disorder transition of the DAPP ligand when the complex converts from the HS to LS state. The oxygen atoms of the perchlorate anions show the values of the anisotropic thermal parameters expected for a fully ordered structure of the counterions.

The HS → LS transition is accompanied by an essential variation of the lattice parameters (Table 1). The volume decrease of the unit cell corresponds to 5.15% (158.4 Å^3) and results from both the lattice parameters' thermal contraction and the shortening of the Fe−N distances upon the spin transition. The network of intermolecular contacts is rather different in the LS structure (Figure 2b). The numerous H-bonds are distributed within a sheet, as well as between the sheets from different layers. Unlike the HS structure, the H-bonds between the molecules belonging to the neighboring sheets inside a layer are fully missing. The two π stacking modes described above for the HS structure are also observed in the LS form. The first one, formed in the *a* direction by the overlapping of the coordinated and noncoordinated abpt pyridyl rings, looks to be slightly affected (Table 5). The

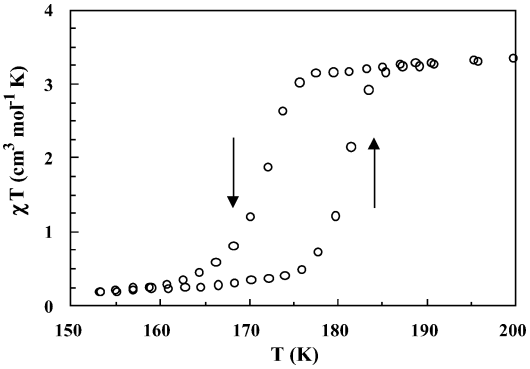

Figure 4. Thermal variation of $\chi_M T$ for [Fe(DAPP)(abpt)]$(ClO_4)_2$.

dihedral angle between the stacked pyridine planes increases to 9.6(2)°. The second π stacking mode, in the *c* direction, involving the noncoordinated pyridyl rings of the abpt ligands, appears significantly weakened (Table 5) at 123 K.

Magnetic Susceptibility Data. The magnetic properties were measured in both cooling and warming modes in order to detect thermal hysteresis effects. The variation of the product of the molar magnetic susceptibility and the temperature $\chi_M T$ versus T is shown in Figure 4. At 295 K, the magnitude of $\chi_M T$ is 3.55 cm^3 mol^{-1} K ($\mu_{eff} = 5.33\ \mu_B$) and corresponds to a quintet spin state. This characteristic value for HS iron(II) complexes varies slightly upon cooling to 176 K, and then an abrupt HS $\rightarrow$ LS transition occurs within 10 K. At 86 K, $\chi_M T$ attains 0.10 cm^3 mol^{-1} K, which is close to the value expected for LS iron (II) complexes. The absence of residual paramagnetism at low temperature evidenced by Mössbauer spectroscopy (vide infra) as well as the closeness of the experimental $\chi_M T$ to the expected value for a pure singlet spin state suggests that the spin transition is practically complete. In the warming mode the spin transition is observed between 176 and 184 K. The observed transition temperatures are $T_c\downarrow = 171$ K and $T_c\uparrow = 181$ K in the cooling and warming modes, respectively, and a hysteresis width is equal to 10 K.

Mössbauer Spectroscopy. The temperature dependent ^{57}Fe Mössbauer spectra of [Fe(DAPP)(abpt)]$(ClO_4)_2$ were studied between 80 and 293 K on cooling and heating. Figure 5 shows five representative spectra (three recorded in the warming and two in the cooling mode) clearly displaying the presence of a hysteresis loop. The values of the Mössbauer parameters obtained by a least-squares fitting are given in Table 6. At 211 K, the Mössbauer spectrum consists of a single doublet with isomer shift $\delta = 1.022(2)$ mm s^{-1} and quadrupole spitting $\Delta E_Q = 1.385(3)$ mm s^{-1}. These parameters are typical of iron(II) in the HS state. In the cooling mode, around 180 K another component appears with the Mössbauer parameters characteristic of the iron(II) LS state. The HS component disappears within a short interval of temperatures ($\sim$5 K) evidencing an abrupt character of the spin transition. At 80 K, the parameters of the spectrum $\delta = 0.570(1)$ mm s^{-1} and $\Delta E_Q = 0.419(1)$ mm s^{-1} are consistent with earlier data for iron(II) LS compounds. At high temperatures ($T > 211$ K), the complete character of the spin transition was confirmed by the absence of a residual LS iron(II) fraction. At 80 K, the spectrum also did not detect

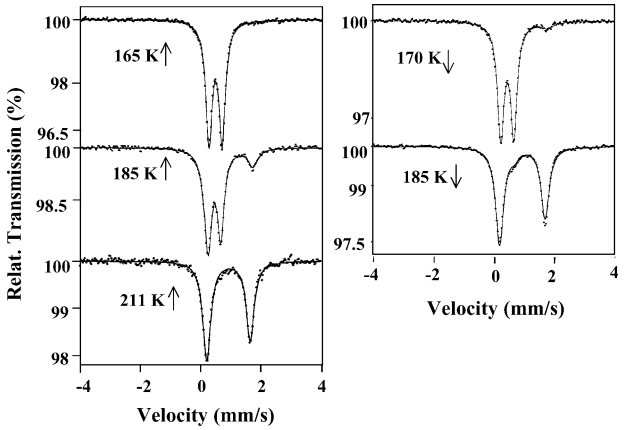

Figure 5. Selected ^{57}Fe Mössbauer spectra of [Fe(DAPP)(abpt)]$(ClO_4)_2$ recorded in the cooling and warming modes. The solid lines represent fitted curves.

any residual HS iron(II) species. The HS fraction (Table 6), n_{HS}, deduced from the ratio A_{HS}/A_{tot} (A_{HS} = area of the HS doublet; A_{tot} = total Mössbauer absorption) evidences, in agreement with magnetic data, the occurrence of an abrupt spin transition around $T_c\downarrow = 176$ K and $T_c\uparrow = 187$ K.

The Mössbauer spectrum of the HS state at 211 K (Figure 5) is clearly dissymmetric. This dissymmetry is not accompanied by any broadening of the lines (the line width $\Gamma \sim 0.31$ mm s^{-1}). A Mössbauer spectral dissymmetry without line broadening may have two possible origins: (i) a texture effect in the sample[1b,20] or (ii) a rapid relaxation of the system between two crystallographically similar configurations with a frequency higher than $\sim 10^8$ s^{-1}.[21] For lower relaxation rates (10^7-10^8 s^{-1}) the dissymmetry is usually accompanied by a line broadening ($\Gamma > 0.4$ mm s^{-1}). To clarify this point, the Mössbauer measurements have been carefully carried out between 185 and 300 K. Figure 6 shows two selected Mössbauer spectra obtained at the same temperature (200 K) with two orientations of the sample *Z*-axis relative to the γ-ray direction: OZ $\parallel \gamma$ and angle (OZ, γ) = 40°. The Mössbauer spectra for both orientations (Figure 6) are similar, confirming the assumption (ii). Thus the presence of the two HS configurations, which may correspond to the two conformations of the DAPP ligand, is suggested at high temperature.

DFT Calculations. The electronic structure calculations were done in order to characterize the influence of the structural disorder above the spin transition temperature on the energy gap between the HS and LS states. The influence of the disordered perchlorate ions cannot be described within isolated-molecule calculations and needs the analysis of the solid as a whole. To study a role of the disorder in the DAPP ligand, only the complex cation was considered in our calculations. Spin transition systems became an object of

(20) Martin, J.-P.; Zarembowitch, J.; Bousseksou, A.; Dworkin, A.; Haasnoot, J. G.; Varret, F. *Inorg. Chem.* **1994**, *33*, 6325.
(21) (a) Hartmann-Boutron, F. *Ann. Phys.* **1975**, *9*, 285. (b) Adler, P.; Hauser, A.; Vef, A.; Spiering, H.; Gütlich, P. *Hyperfine Interact.* **1989**, *47*, 343. (c) Adler, P.; Spiering, H.; Gütlich, P. *J. Chem. Phys.* **1989**, *50*, 587. (d) Bousseksou, A.; Place, C.; Linares, J.; Varret, F. *J. Magn. Magn. Mater.* **1992**, *104−107*, 225. (e) Lemercier, G.; Bousseksou, A.; Verelst, M.; Varret, F.; Tuchagues, J. P. *J. Magn. Magn. Mater.* **1995**, *150*, 227.

Table 6. Least-Squares-Fitted Mössbauer Data[a,b] in the Heating (↑) and Cooling (↓) Modes for [Fe(DAPP)(abpt)]$(ClO_4)_2$

	low-spin state			high-spin state			
T (K)	δ (mm·s^{-1})	ΔE_Q^{LS} (mm·s^{-1})	Γ (mm·s^{-1})	δ (mm·s^{-1})	ΔE_Q^{HS} (mm·s^{-1})	Γ (mm·s^{-1})	A_{HS}/A_{tot} (%)
80↑	0.570(1)	0.419(1)	0.254(1)				0
180↑	0.544(2)	0.404(2)	0.268(2)				0
185↑	0.548(1)	0.397(2)	0.258(1)	1.012(4)	1.528(9)	0.356(7)	22.3(6)
190↑	0.7(2)	*0.4*	0.54(6)	1.038(1)	1.443(2)	0.290(2)	89(1)
211↑				1.022(1)	1.385(2)	0.306(2)	100(0)
185↓	*0.54*	*0.47*	0.312(2)	1.043(1)	1.452(2)	0.312(1)	91.2(4)
180↓	0.508(1)	0.54(2)	0.314(2)	1.055(2)	1.451(3)	0.314(2)	84.0(6)
170↓	0.549(1)	0.417(1)	0.246(1)	1.15(2)	1.34(3)	0.55(3)	9.5(8)

[a] δ, isomer shift; ΔE_Q, quadrupole splitting; Γ, half-height width of line; A/A_{tot}, area ratio. [b] Statistical standard deviations are given in parentheses; isomer shift values refer to metallic iron at 300 K; italicized values were fixed during the fitting procedure.

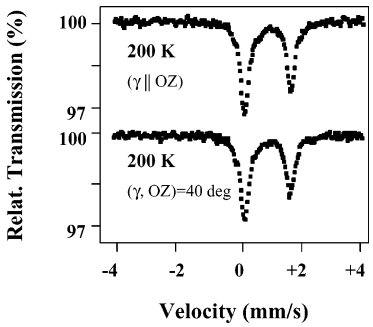

Figure 6. ^{57}Fe Mössbauer spectra of [Fe(DAPP)(abpt)]$(ClO_4)_2$ recorded for two orientations of the sample *Z*-axis relative to the γ-ray direction: OZ ∥ γ and angle (OZ, γ) = 40° at 200 K.

quantum chemical DFT research only in the past few years,[22] and presently there is no commonly accepted methodology for calculations of the HS−LS energy gap and vibrational frequencies in two spin states. If some studies propose the B3LYP method as a best tool for calculations of the energy gap,[22a−c] for some systems more reasonable results were found with BLYP and PW 91 methods,[22d] or with a recently proposed reparametrized hybrid functional.[17] In this work, our goal was not to reproduce numerically the splitting between two spin multiplets, but rather to study qualitatively the influence of the disorder in the ligand on the spin transition. The single-point calculations of the HS and LS states were performed for the structure found at 123 K, as well as for two structures, corresponding to the two configurations of the DAPP ligand, observed at 293 K. We checked four different exchange-correlation functionals. All functionals correctly predict the LS ground state for the 123 K structure. But only one of them, namely, the hybrid B3LYP functional, gives the HS ground state for the geometry at 293 K. So, we consider the results obtained with this functional as the most credible. The calculations give $\Delta E = E^{293}{}_{LS} - E^{293}{}_{HS}$ equal to 32.7 and 37.7 kJ/mol for the two conformations with C21A and C21B, respectively. The obtained energy gaps do not describe the difference between the two states at their equilibrium geometries, which can be found only from calculations with the structure optimization. The excited LS state lies closer to the ground HS state for the methylene group in the C21A position, clearly displaying the importance of the DAPP configuration for the modulation of the singlet−quintet gap. It means that this configuration favors the transition into the LS state. The preference of the LS state in this case follows from the crystal field variation. The Mulliken charges at the N2 atom in the excited LS state are equal to −0.640 and −0.547 in the configurations A and B, respectively. The charges of other nitrogen atoms vary only slightly. Thus, the configuration A corresponds to a stronger effective ligand field. One can suppose that the ordering at lower temperatures of the DAPP ligand in this configuration presumably promotes the spin transition.

Discussion

This work was initially undertaken to design a new binuclear iron(II) cooperative spin crossover system. This goal dictated a choice of polydentate ligands providing nitrogen donor atoms. The commercial 4-amino-3,5-bis-(pyridin-2-yl)-1,2,4-triazole (abpt) was selected as a bis-bidentate bridging ligand able to maintain two metal ions in the complex.[23] Moreover, the abpt ability to form spin crossover compounds is known in the literature.[18c,e,f] The octahedral coordination sphere of iron(II) was completed with the DAPP tetradentate ligand. Our synthetic strategy of the design of new spin transition systems rests on the use of the polydentate ligands with mixed aliphatic and aromatic nitrogen atom functions featuring an intermediate ligand field force.[3,24] We also kept in mind that the involvement of amino and pyridyl groups in the structure of both abpt and DAPP ligands may effect favorably the generation of intermolecular H-bonding and/or π stacking interactions leading to cooperative effects. In this context, we endeavored to obtain a binuclear complex, using the ratio of initial components as $Fe(ClO_4)_2$:DAPP:abpt = 2:2:1. However, the formation of a binuclear compound failed, probably because of the steric hindrance from the close coordination of two tetradentate

(22) (a) Bolvin, H. *J. Phys. Chem A* **1998**, *102*, 7525. (b) Paulsen, H.; Winkler, H.; Trautwein, A. X.; Grünsteudel, H.; Rusanov, V.; Toftlund, H. *Phys. Rev. B* **1999**, *59*, 975. (c) Chen, G.; Espinoza-Perez, G.; Zentella-Dehesa, A.; Silaghi-Dumitrescu, I.; Lara-Ochoa, F. *Inorg. Chem.* **2000**, *39*, 3440. (d) Paulsen, H.; Duelund, L.; Winkler, H.; Toftlund, H.; Trautwein, A. X. *Inorg. Chem.* **2001**, *40*, 2201. (e) Schmiedecamp, A. M.; Ryan, M. D.; Deeth, R. J. *Inorg. Chem.* **2002**, *41*, 5733. (f) Brehm, G.; Reiher, M.; Schneider S. *J. Phys. Chem. A* **2002**, *106*, 12024.

(23) (a) Keij, F. S.; de Graaff, R. A. G.; Haasnoot, J. G.; Reedijk, J. *J. Chem. Soc., Dalton Trans.* **1984**, 2093. (b) van Königsbruggen, P. J.; Gatteschi, D.; de Graaff, R. A. G.; Haasnoot, J. G.; Reedijk, J.; Zanchini, C. *Inorg. Chem.* **1995**, *34*, 5175.

(24) Matouzenko, G. S.; Bousseksou, A.; Lecocq, S.; Koningsbruggen, P. J. v.; Perrin, M.; Kahn, O.; Collet, A. *Inorg. Chem.* **1997**, *36*, 2975.

ligands. Under these experimental conditions, a new mononuclear cooperative spin crossover compound, [Fe(DAPP)(abpt)]$(ClO_4)_2$, was isolated instead.

The presence of the pronounced hysteresis of width 10 K evidenced a first-order character of the spin crossover in [Fe(DAPP)(abpt)]$(ClO_4)_2$. This cooperative spin transition does not arise from the crystallographic phase transition, and the monoclinic space group $P2_1/n$ is retained in both spin state isomers. The explanation of strong cooperativity must be sought in the intrinsic structural features of the complex. The X-ray analysis displays the two main characteristics: a branched network of intermolecular links in the crystal lattice and the occurrence of two types of order−disorder transitions accompanying the thermal spin change.

We believe the dense network of intermolecular interactions to be crucial for a strongly cooperative behavior of spin transition in [Fe(DAPP)(abpt)]$(ClO_4)_2$. The intermolecular interactions are represented by the hydrogen bound and the π stacked networks. Let us consider them in both HS and LS structures. At room temperature, each molecule participates in the formation of thirteen H-bonds (Table 4), including the five intramolecular and the eight intermolecular ones. Among the latter, the four H-bonds involve the nitrogen atoms directly linked to the iron(II) ion. The two bifurcated H-bonds, i.e., N(3)−H(3A)···O(21) and N(3)−H(3B)···O(21) (Figure 2a), link the molecules from two different sheets inside a layer in the two-dimensional H-bound network (parallel to the *ac* plane). The corresponding Fe−Fe distance (7.950(2) Å) is rather short in comparison with other mononuclear spin-crossover systems.[3b,25] The two O21 atoms from two perchlorate ions, related by the symmetry operation $-x, -y, -z$, can be seen like a "di-μ-oxo bridge" coupling the two molecules. These H-bonds can be considered of key importance for the cooperativity in the HS complex. We also identified the two modes of π stacking interaction in the 293 K structure (Table 5). The overlap between the coordinated and noncoordinated pyridyl rings of the abpt ligands (Figure 3) links the complexes in the linear chains along the *a* direction. The Fe−Fe distance in the chain of π stacked molecules is equal to 9.425(2) Å. The second mode, via the stacking of both noncoordinated pyridyl rings of the abpt ligands from the molecules in different sheets inside a layer, runs in the *c* direction. It can be seen (Figure 3) that the noncoordinated pyridyl ring of each abpt ligand participates simultaneously in both modes of π stacking interaction. However, the Fe−Fe separation in the second mode is rather high 15.755(4) Å. Summarizing, both H-bonding and π stacking spread in the HS crystal structure inside layers parallel to the *ac* plane forming a strongly cooperative two-dimensional network of molecules. By contrast, the two-sheet layers are connected in the *b* direction mainly by weaker van der Waals interactions.

The thermal spin transition is attended by a considerable change of the lattice parameters (Table 1). At 123 K, the anisotropy in the unit cell variation corresponds to 0.9%, 2.6%, and 7.5% for the *a*, *b*, and *c* axes, respectively. In particular, *a* and *b* increase, whereas the *c* parameter decreases significantly. The β angle value also increases by 3.4%. These drastic changes impose the modifications in the molecular crystal packing and, accordingly, in the system of intermolecular interactions. In the LS complex the number of H-bonds increases (Table 4), but their spreading in the crystal lattice is quite different (Figure 2). Now the H-bonds can be regarded as intrasheet and interlayer intermolecular contacts via the oxygen atoms of perchlorate anions. The corresponding Fe−Fe distance, which was as short as 7.950(2) Å in the HS form, equals 9.014(2) Å in the LS structure. No more intersheet H-bonds inside a layer are observed. As far as the π stacking network is concerned, the first mode (in the *a* direction) is rather similar (Table 5) with the close Fe−Fe distance of 9.511(2) Å. The second mode, in the *c* direction, changes considerably. Only a few intermolecular C···C contacts are observed (Table 5), although the Fe−Fe distance decreases (13.879(3) Å). Thus, a total weakening of π stacking interactions in the LS structure may be expected. It is readily seen that the modification in the propagation of intermolecular interactions fully correlates with the anisotropy of lattice parameters variations on cooling.

The obtained value of the hysteresis loop width (∼10 K) seems quite high for mononuclear spin-transition compounds. To the best of our knowledge, the only example of a mononuclear spin crossover system showing an essentially larger hysteresis (40 K) that has been structurally characterized in both the HS and LS states is [Fe(PM-PEA)$_2$(NCS)$_2$] (PM-PEA = *N*-(2′-pyridylmethylene)-4-(phenylethynyl)-aniline).[25c] However, the hysteresis effect for the latter compound is connected with a crystallographically significant structural phase transition. It is very likely that the pronounced hysteresis in our case, without any crystallographic phase transition, originates from the dramatic change of the unit cell parameters (Table 1) and rearrangement of the cooperative interaction topology (Figures 2 and 3).

The second striking result of the present study is the occurrence of the two order−disorder transitions that accompany the spin change. It should be noted that the role of order−disorder phenomena has been discussed in the spin crossover literature for a long time. So far, only the disorder of noncoordinated to iron(II) atom species, counteranions[26] and solvent molecules,[26f,27] has been observed in spin transition complexes. For the first time, the disorder was suggested to be related to the nature of the spin transition for [Fe(2-

(25) (a) Gallois, B.; Real, J. A. Hauw, C.; Zarembowitch, J. *Inorg. Chem.* **1990**, *29*, 1152. (b) Létard, J.-F.; Guionneau, P.; Rabardel, L.; Howard, J. A. K.; Goeta, A. E.; Chasseau, D.; Kahn, O. *Inorg. Chem*. **1998**, *37*, 4432. (c) Guionneau, P.; Létard, J.-F.; Yufit, D. S.; Chasseau, D.; Bravic, G.; Goeta, A. E.; Howard, J. A. K.; Kahn, O. *J. Mater. Chem*. **1999**, *9*, 985.

(26) (a) König, E.; Ritter, G.; Kulshreshtha, S. K.; Nelson, S. M. *Inorg. Chem*. **1982**, *21*, 3022. (b) Fleisch, J.; Gütlich, P.; Hasselbach, K. M.; Müller, W. *Inorg. Chem*. **1976**, *15*, 958. (c) Weihl, E. *Acta Crystallogr., Sect. B* **1993**, *49*, 289. (d) Breuning, E.; Ruben, M.; Lehn, J.-M.; Renz, F.; Garcia, Y.; Ksenofontov, V.; Gütlich, P.; Wegelius, E.; Rissanen, K. *Angew. Chem., Int. Ed.* **2000**, *39*, 2504. (e) Holland, J. M.; McAllister, J. A.; Lu, Z.; Kilner, C. A.; Thornton-Pett, M.; Halcrow, M. A. *Chem. Commun.* **2001**, *577*. (f) Matouzenko, G. S.; Molnar, G.; Bréfuel, N.; Perrin, M.; Bousseksou, A.; Borshch, S. A. *Chem. Mater*. **2003**, *15*, 550.

pic)$_3$]Cl$_2$·EtOH (2-pic = 2-(aminomethyl) pyridine).[27a] On the basis of the X-ray data at three temperatures, the thermal ordering of the ethanol molecule, interacting with the complex [Fe(2-pic)$_3$]Cl$_2$ through hydrogen bonds, has been considered as a trigger of the spin transition. Some years later, the order−disorder phenomenon was examined by Mössbauer spectroscopy for [Fe(dppen)$_2$Cl$_2$]·2(CH$_3$)$_2$CO (dppen = *cis*-1,2-bis(diphenylphosphino)ethylene).[27d] The ordering of the acetone molecules was similarly proposed as an initiator of the spin transition. Well after, the X-ray study at two temperatures was performed for the analogous complex with chloroform [Fe(dppen)$_2$Br$_2$]·2CHCl$_3$ and likewise the HS to LS conversion of complex was supposed to be influenced by the order−disorder transformation of the solvent molecules.[27h] In several spin crossover systems the order−disorder phenomena manifest themselves in the Mössbauer spectral lines splitting.[26a,28] As in previously studied examples, we identified an order−disorder transition involving the counterions. The perchlorate anions with Cl2 atom, being disordered over two orientations with the 0.5:0.5 population ratio at 293 K, are ordered in one preferential orientation at 123 K. It is appropriate to recall that only this perchlorate ion via the O21 atom participates in the H-bonds, which are presumed to be of primary importance for the cooperative interactions in the complex. Moreover, the comparison of N(3)−H(3A)···O(21)/O(21A) and N(3)−H(3B)···O(21)/O(21A) distances (Table 4) at 293 and 183 K shows their overall decrease on cooling, suggesting that the ordering of the perchlorate ions strengthens the cooperative interactions via hydrogen bonding.

[Fe(DAPP)(abpt)](ClO$_4$)$_2$ gives, to the best of our knowledge, the first example of a spin crossover system with the order−disorder transition, involving the ligand directly coordinated to the iron(II) site. As it follows from the DFT calculations, two conformations of the DAPP ligand result in slightly different values of the HS−LS gap. The dissymmetry observed in the Mössbauer spectra may arise from the relaxation between these two configurations. The ligand conformation that is preferentially populated at low-temperature corresponds to a less important value of the energy splitting and thus favors the crossing between the LS and HS states. So, in line with previous studies the order−disorder phenomena and spin transition in [Fe(DAPP)(abpt)](ClO$_4$)$_2$ seem to be internally interrelated. One may suppose that both tuning of the ligand field strength by the DAPP ligand and reinforcement of the cooperative interactions due to the thermal ordering in the perchlorate ions provide an intrinsic impulse for the initiation of the spin transition in [Fe(DAPP)(abpt)](ClO$_4$)$_2$.

It can be noted that the order−disorder transitions in both the ligand and the perchlorate anion can be interconnected. Our attempts to reproduce two configurations of the ligand by the DFT calculations of the free complex cation were unsuccessful. The structure optimization procedure, started from the two experimentally observed ligand configurations, converged to a single molecular geometry, suggesting that the ligand disorder has a lattice origin. Further experimental studies, especially heat capacity measurements, are under way now.

Finally, to examine the role of counterions, the compounds [Fe(DAPP)(abpt)]X$_2$ with X = BF$_4$, PF$_6$ were also prepared. Their magnetic behavior shows that the nature of the counterion plays an important role in the spin transition regime of [Fe(DAPP)(abpt)]X$_2$. The complex with the tetrahedral (like in the case of ClO$_4$) BF$_4$ anion displays magnetic behavior similar to that of [Fe(DAPP)(abpt)](ClO$_4$)$_2$ with the hysteresis loop slightly displaced toward higher temperatures. In contrast, the complex with the octahedral PF$_6$ anion shows a gradual spin transition, shifted toward lower temperatures, without hysteresis. The investigation of the interrelation of the magnetic properties and structure, perturbed by the nature of noncoordinated anion, is in progress.

Acknowledgment. We are indebted to Professor M. Sorai for very valuable comments. We also thank J.-F. Meunier for technical assistance.

Supporting Information Available: A full presentation of crystallographic data and experimental parameters, atomic positional parameters, anisotropic displacement parameters, and bond lengths and angles in CIF format. This material is available free of charge via the Internet at http://pubs.acs.org.

IC034450E

(27) (a) Mikami, M.; Konno, M. Saito, Y. *Chem. Phys. Lett*. **1979**, *63*, 566. (b) Katz, B. A.; Strouse, C. E. *J. Am. Chem. Soc*. **1979**, *101*, 6214. (c) Mikami, M.; Konno, M.; Saito, Y. *Acta Crystallogr., Sect. B* **1980**, *36*, 275. (d) König, E.; Ritter, G.; Kulshreshtha, S. K.; Waigel, J.; Sacconi, L. *Inorg. Chem*. **1984**, *23*, 1241. (e) Weihl, L.; Kiel, G.; Köhler, C. P.; Spiering, H.; Gütlich, P. *Inorg. Chem*. **1986**, *25*, 1565. (f) Conti, A. J.; Chadha, R. K.; Sena, K. M.; Rheingold, A. L.; Hendrickson, D. N. *Inorg. Chem*. **1993**, *32*, 2670. (g) Conti, A. J.; Kaji, K.; Nagano, Y.; Sena, K. M.; Yumoto, Y.; Chadha, R. K.; Rheingold, A. L.; Sorai, M.; Hendrickson, D. N. *Inorg. Chem*. **1993**, *32*, 2681. (h) Wu, C.-C.; Jung, J.; Gantzel, P. K.; Gütlich, P.; Hendrickson, D. N. *Inorg. Chem*. **1997**, *36*, 5339.

(28) Poganiuch, P.; Decurtins, S.; Gütlich, P. *J. Am. Chem. Soc*. **1990**, *112*, 3270.